Effects of Radar Proximity on Single-Doppler Velocity Signatures of Axisymmetric Rotation and Divergence

VINCENT T. WOOD AND RODGER A. BROWN

NOAA, Environmental Research Laboratories, National Severe Storms Laboratory, Norman, Oklahoma

(Manuscript received 23 July 1991, in final form 3 March 1992)

ABSTRACT

Geometrical and mathematical relationships are developed to explain the variation with radar range of idealized single-Doppler velocity patterns of axisymmetric rotation and divergence regions. The velocity patterns become distorted as they approach a Doppler radar site. As a consequence, the apparent core diameters and locations of the centers of the features depart from the true values. Equations are derived to estimate the true values from the distorted Doppler velocity fields.

1. Introduction

During the past several decades, Doppler radars have been used to measure flow within a variety of atmospheric phenomena. Because they measure only a one-dimensional radial component of three-dimensional flow that varies as a function of azimuth, elevation, and time, Doppler velocity measurements are not straightforward to interpret. Therefore, one resorts to the use of Doppler velocity pattern, or signature, recognition to interpret the measurements (e.g., Donaldson 1970; Wilson and Wilk 1982; Wood and Brown 1986; Brown and Wood 1991). Two important Doppler velocity signatures are those produced by quasi-axisymmetric rotation and divergence regions. Examples of these signatures are mesocyclone signatures associated with strong, rotating updraft cores within some severe thunderstorms (e.g., Burgess 1976), mesoscale vortex signatures associated with mesoscale convective systems (e.g., Houze et al. 1989), hurricane vortex signatures associated with large hurricane circulations (e.g., Baynton 1979; Wood and Marks 1989), and divergence signatures associated with strong divergent outflows near storm top (e.g., Lemon and Burgess 1980; Witt and Nelson 1991) and with low-altitude microbursts (e.g., Wilson et al. 1984; Fujita 1985; Eilts and Doviak 1987).

Doppler velocity signatures vary as a function of range from the radar. At far range, it is the width of the radar beam (which increases linearly with range) that causes the degradation of the peak velocities in phenomena such as the thunderstorm mesocyclone. Problems arise when the beamwidth approaches the core diameter in azimuthal extent (e.g., Donaldson 1970; Brown et al. 1978).

A different problem arises at short range. The signatures of axisymmetric rotation and divergence become distorted as the features move within several core diameters of the radar. As a result, it becomes difficult to determine the true core diameter and center location of the feature. This situation is especially important with a hurricane approaching a shoreline radar, where the range to the circulation center can be in error by a significant fraction of the true range. In Brown and Wood (1991), we briefly discussed the effect of close range on signatures, but did not present mathematical and geometrical relationships to explain such variations.

In this paper, we limit our attention to the distortion of Doppler velocity signatures at short range from a radar, with an emphasis on geometrical, as well as mathematical, information on the variation of signatures of axisymmetric rotation and divergence with radar range. In section 2, the development and mathematical specifications of flow models are presented. For this investigation, only three flow models are used: axisymmetric rotational (tangential) flow about a vertical axis, axisymmetric divergence (flowing radially outward from a central point), and a mix of axisymmetric rotational and divergent flow fields. The phenomenon being given primary consideration is a hurricane. In section 3, mathematical and geometrical expressions are developed to explain the variation in the single-Doppler velocity patterns of axisymmetric rotation and divergence regions as a function of radar range. In section 4, expressions are developed for estimating the true core diameter of an axisymmetric flow field and its true distance from the radar based on the measured quantities. These expressions are applied to two atmospheric flow situations in section 5. Conclusions and

Corresponding author address: Vincent T. Wood, NOAA/ERL/NSSL, 1313 Halley Circle, Norman, OK 73069.

future research concerns are discussed in sections 6 and 7, respectively. Readers not interested in the detailed mathematical developments can skip sections 2 and 4.

2. Doppler velocity values for axisymmetric flow fields

Many of the basic horizontal flow fields within hurricanes, mesoscale convective systems, and thunderstorms can be specified, to a first approximation, by axisymmetric velocity distributions (e.g., Shea and Gray 1973; Gray and Shea 1973; Brown and Wood 1983, 1991). It is possible to simulate the basic flow features using simple analytical flow models. The Rankine-combined velocity profile (Rankine 1901), which is symmetric about a vertical axis, can be used to specify both axisymmetric rotation and axisymmetric divergence. According to the profile, tangential- and radial-velocity components increase linearly from a circulation or divergence center (where velocity is zero) to a core radius where the velocity attains its maximum value. Beyond the core radius, the velocity is inversely proportional to distance from the center. Furthermore, for combinations of rotational and divergent flow, we assume that the two flow-field components have the same core radius and a common vertical axis. (Examples of these various flow fields and their Doppler velocity signatures are shown in Fig. 1.)

Mathematically, the velocity distributions for radial, $v_r(r)$, and tangential, $v_t(r)$, wind components in the Rankine model are given by

$$v_r(r) = V_r\left(\frac{r}{r_c}\right)^{\lambda}, \quad (1)$$

$$v_t(r) = V_t\left(\frac{r}{r_c}\right)^{\lambda}, \quad (2)$$

where V_r is the peak radial velocity at the core radius r_c, V_t is the peak tangential velocity at r_c, and r is the distance from the flow-feature center. The exponent λ describes the radial profile of radial and tangential wind components. For the simulations presented here, we assume that $\lambda = 1$ for $r \leq r_c$ and that $\lambda = -1$ for $r > r_c$.

The Doppler velocity component V_d at range R_d is the component of the wind vector in the viewing direction θ_d from the radar. As derived in appendix A, the Doppler velocity value at R_d, θ_d is given by

$$V_d = \left(\frac{r}{r_c}\right)^{\lambda-1}\left\{V_r\left[\frac{R_d}{r_c} - \frac{R_T}{r_c}\cos(\theta_d - \theta_T)\right] + V_t\frac{R_T}{r_c}\sin(\theta_d - \theta_T)\right\}, \quad (3)$$

where R_T and θ_T are the range and azimuth of the true flow-feature center from the radar. Simulated Doppler velocity fields are generated by the flow models described in (1) and (2). We use a right-hand orthogonal coordinate system with the origin at the center of the

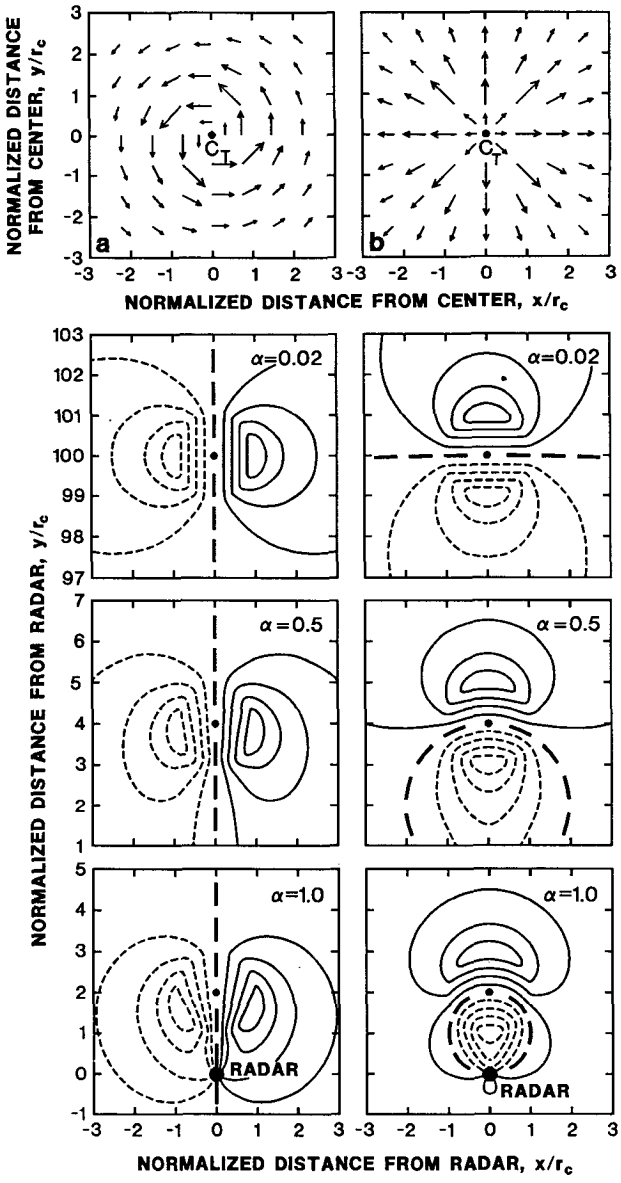

FIG. 1. Horizontal (a) vortex and (b) divergence flow fields. The wind-vector length is proportional to wind speed. The true circulation center C_T is indicated by the small black dot at the center of each panel. Variations of axisymmetric (a) vortex and (b) divergence Doppler velocity signatures as a function of distance north of the radar are shown beneath the respective flow fields. Solid curves represent flow away from the radar (positive Doppler velocities), short dashed curves represent flow toward the radar (negative Doppler velocities), and the thick, long-dashed curve represents flow normal to the radar viewing direction (zero Doppler velocities). Doppler velocity values are normalized relative to the peak wind-speed value with contour intervals of 0.2. Radar is located at 100, 4, and 2 core radii south of the flow field (aspect ratios of 0.02, 0.5, and 1.0, respectively). Distances in the x and y directions have been normalized by the core radius r_c. In the last two panels, radar location is indicated by the large black dot (adapted from Brown and Wood 1991).

grid; we assume that the grid origin (0, 0) represents the center of flow feature and that the true range to the grid origin is given by R_T. Given the variables V_r, V_t, r_c, λ, R_T, and θ_T, the distance r from the flow-feature center is computed at Cartesian (x, y) grid points in a horizontal analysis plane. The range R_d from the radar to a specific grid point is given by

$$R_d(x, y, R_T, \theta_T) = [(x + R_T \sin\theta_T)^2 + (y + R_T \cos\theta_T)^2]^{1/2}. \quad (4)$$

Here θ_d is defined as the angle (positive in a clockwise direction) at the radar location between north and the grid point, and is given by

$$\theta_d = \tan^{-1}\left(\frac{x + R_T \sin\theta_T}{y + R_T \cos\theta_T}\right). \quad (5)$$

Thus, the Doppler velocity value V_d at a grid point is calculated from (3). Simulated Doppler velocity fields contain some additional simplifying assumptions. The vertical component of motion is not simulated; therefore, the radar measurements are assumed to be made at low-elevation angles. Furthermore, the simulation assumes that the radar measurements are free of noise and that the radar beam has an infinitesimal width (producing perfect radar resolution at all ranges).

3. Pattern change at short range

The Doppler velocity pattern is a function of the core diameter and the range of the feature center from the radar. Thus, it is convenient to categorize Doppler velocity patterns in terms of a dimensionless aspect ratio α that is defined as

$$\alpha \equiv \frac{\text{core diameter}}{\text{range to center}} = \frac{D_T}{R_T}, \quad (6)$$

where the subscript T represents the true value of the parameter.

Figure 1 shows how the axisymmetric rotation and divergence signatures vary as a function of range from the radar (e.g., Brown and Wood 1991). The signature consists of a symmetric couplet of closed contours representing opposite Doppler velocity values. With decreasing range from the radar (i.e., α increases), the Doppler velocity patterns within the signatures become distorted relative to the patterns at farther range.

a. Axisymmetric rotation

The Doppler velocity pattern for axisymmetric cyclonic rotation is shown in Fig. 2a, wherein the pattern was computed for a signature center location at one core diameter ($2r_c$) from the radar ($\alpha = 1.0$). The distortion of the pattern owing to increased proximity to the radar (Fig. 1) can be explained by setting the radial component V_r to zero in (3). Doppler velocity V_d normalized by the peak tangential V_t velocity at the edge of the core region is given by

$$\frac{V_d}{V_t} = \frac{2}{\alpha}\left(\frac{r}{r_c}\right)^{\lambda-1} \sin(\theta_d - \theta_T), \quad (7)$$

where $R_T/r_c = 2/\alpha$ is the varied parameter in this

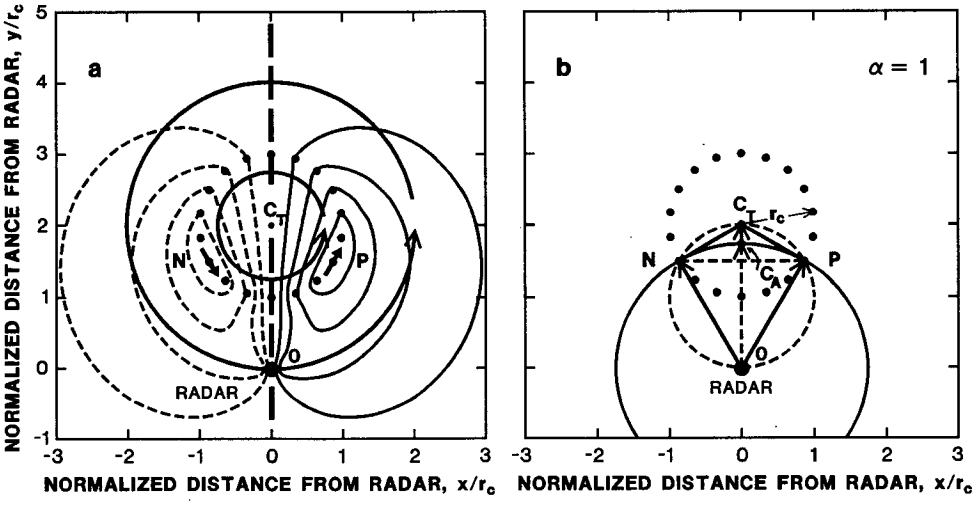

FIG. 2. (a) Plan view of axisymmetric vortex flow (thicker streamlines) and corresponding single-Doppler velocity signature (thinner curves) for a radar located at one core diameter south of the flow field ($\alpha = 1$). Doppler velocity contour convention is the same as in Fig. 1. Heavy arrows at points N and P represent peak tangential velocities at the core radius r_c. (b) Geometrical relationships between Doppler radar location O, true circulation center C_T, and locations of the extreme positive (P) and negative (N) Doppler velocity values. The apparent circulation center is C_A. The solid circle is the radar range circle through N and P; the dashed chord NP represents apparent diameter D_A of the vortex.

study. When λ is chosen to be +1 (pure solid-body rotation) in (2), radar r dependence disappears, and thus, Doppler velocity isolines within the core region of axisymmetric rotation are parallel to the radar viewing direction for all aspect ratios. With decreasing range, the isolines become increasingly skewed relative to the nearly parallel isolines at far range. For any value of Doppler viewing direction θ_d relative to the true azimuth θ_T of the circulation center C_T, the isolines within the core region are equally spaced at constant range. Outside the core region, the isolines on the radar side of the vortex signature tend to increasingly converge toward the radar location as the aspect ratio increases.

As indicated in Fig. 2b, the peak Doppler velocity values are at N and P on the dotted circle of maximum winds centered on the true circulation center C_T. The dashed circle passing through the radar O and N and P also passes through the true circulation center C_T; OC_T is the diameter of the circle. In this case of pure axisymmetric rotation, the two Doppler velocity peaks are at the same range (solid circle) from the radar. Note in Fig. 2b that the true circulation center C_T is at a greater range than points N and P.

The true range R_T of the true circulation center C_T from the radar is defined as the dashed length OC_T, which is the diameter of the dashed circle for pure axisymmetric rotation (Fig. 2b) and a chord of the circle for other flow fields (Figs. 3b and 4b). The apparent diameter D_A is defined as the length of the dashed line NP. The apparent circulation center C_A could simply have been defined as the midpoint of line segment NP. We found, however, that the derivations of subsequent mathematical functions were simplified when we defined the apparent circulation center to be at the average range of the velocity peaks (N, P) and to lie along the bisector of the radar viewing angle between the velocity peaks ($\angle NOP$).

b. Divergent rotation

For a divergent vortex, the Doppler velocity is given by

$$\frac{V_d}{V_t} = \left(\frac{r}{r_c}\right)^{\lambda-1}\left\{\frac{V_r}{V_t}\left[\frac{R_d}{r_c} - \frac{2}{\alpha}\cos(\theta_d - \theta_T)\right] + \frac{2}{\alpha}\sin(\theta_d - \theta_T)\right\}, \quad (8)$$

where R_d is the range from the radar to the point in space where the equation is evaluated and V_r/V_t is the ratio of peak radial to peak tangential velocity. For the example shown in Fig. 3, the velocity ratio is 0.5. The effect of adding axisymmetric divergence ($V_r > 0$) to axisymmetric rotation is a counterclockwise shift of the peaks (N and P) and distortion of the Doppler velocity patterns (Fig. 3a) relative to rotation alone (Fig. 2a); the amount of shift is a function of the ratio of peak radial velocity V_r to peak tangential velocity V_t. The dashed circle that passes through the radar location O, the divergent rotation center C_T, and the locations of extreme Doppler velocity values (N, P) shifts to the right and increases in size. The dashed length OC_T is no longer a diameter of the dashed circle; it has become a chord. If convergence instead of divergence (same magnitude) had been added to pure rotation, the figures corresponding to Fig. 3 would be mirror images relative to the line passing through the radar and the true center of the flow feature.

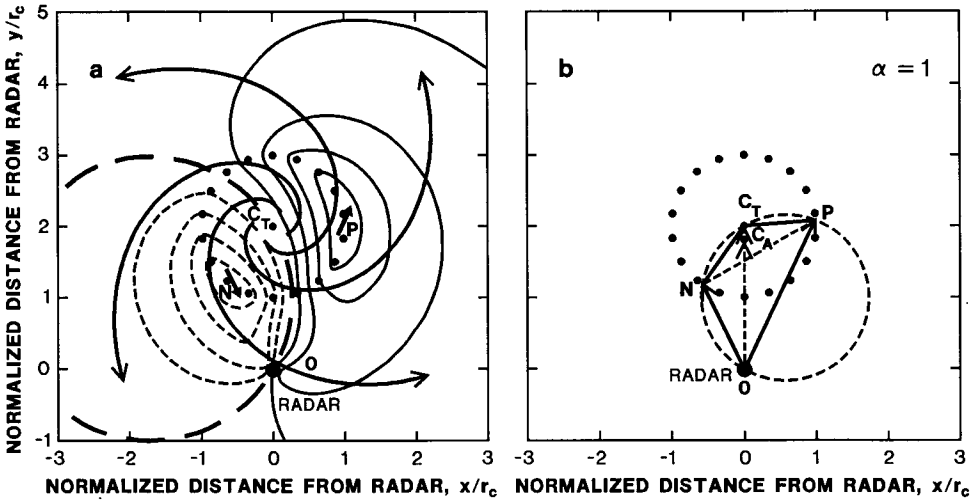

FIG. 3. Same as Fig. 2 except that divergence is added to cyclonic rotation and the solid circle representing radar range circle through N and P is removed. Axisymmetric divergent vortex flow is indicated by thick streamlines.

c. Axisymmetric divergence

The axisymmetric divergence signature centered one core diameter from the radar is shown in Fig. 4a. Setting the tangential component V_t to zero in (3), the Doppler velocity is given by

$$\frac{V_d}{V_r} = \left(\frac{r}{r_c}\right)^{\lambda-1}\left[\frac{R_d}{r_c} - \frac{2}{\alpha}\cos(\theta_d - \theta_T)\right]. \quad (9)$$

The zero Doppler velocity contour ($V_d = 0$) represents flow perpendicular to the radar viewing direction and is a circle of diameter OC_T that passes through the divergence center and radar location; since $2/\alpha = R_T/r_c$, this occurs when $R_d = R_T\cos(\theta_d - \theta_T)$. Within the core of the axisymmetric divergence region ($\lambda = +1$), the Doppler velocity isolines are normal to the radar viewing direction for all aspect ratios. As indicated in Fig. 1, the isolines within the core region become increasingly curved with decreasing range.

As the flow field varies from pure rotation to pure divergence, the dashed circle shifts to the right and becomes infinitely large, as can be seen in Figs. 2b–4b. At the same time, the chord NP of the dashed circle rotates until it becomes collinear with OC_T. The true (C_T) and apparent (C_A) centers of a divergence signature are coincident, independent of distance from the radar.

d. Variation of signature with aspect and velocity ratios

The location of the apparent center C_A varies with both the aspect ratio α and the ratio of peak radial velocity to peak tangential velocity V_r/V_t. These relationships are illustrated in Fig. 5. At a fixed velocity ratio (Fig. 5a), the apparent center moves progressively away from the true center C_T with increasing proximity of the nondivergent vortex signature to the radar (as indicated by heavy arrows). At the same time, the chords NP, which are parallel for all aspect ratios, decrease in length (apparent diameter) with increased proximity.

As the flow field changes from pure rotation ($V_r/V_t = 0$) to pure divergence ($V_r/V_t = \infty$) in Fig. 5b, the apparent center for a fixed aspect ratio moves progressively toward the true center until it becomes collocated with the true center for pure divergence (as indicated by the straight arrow). At the same time, the chords NP rotate in a counterclockwise direction (as indicated by curved arrows) and pass through a common point K on the radial through the true center.

4. Estimation of true core diameter and center location

In section 3, we showed that the Doppler velocity signatures for rotation, divergent rotation, and divergence vary as a function of range from the radar. In this section, we derive analytical expressions for estimating the true diameter from the apparent diameter D_A of the signature, and for estimating the true center from the apparent location of the signature center (R_A, θ_A) relative to the radar.

For various combinations of axisymmetric rotation and divergence, the radar viewing direction at low elevation angles is parallel to the horizontal flow at two points around the edge of the core region. Thus, the true peak flow at the edge of the core region always is measured at the locations of the peak Doppler velocity values.

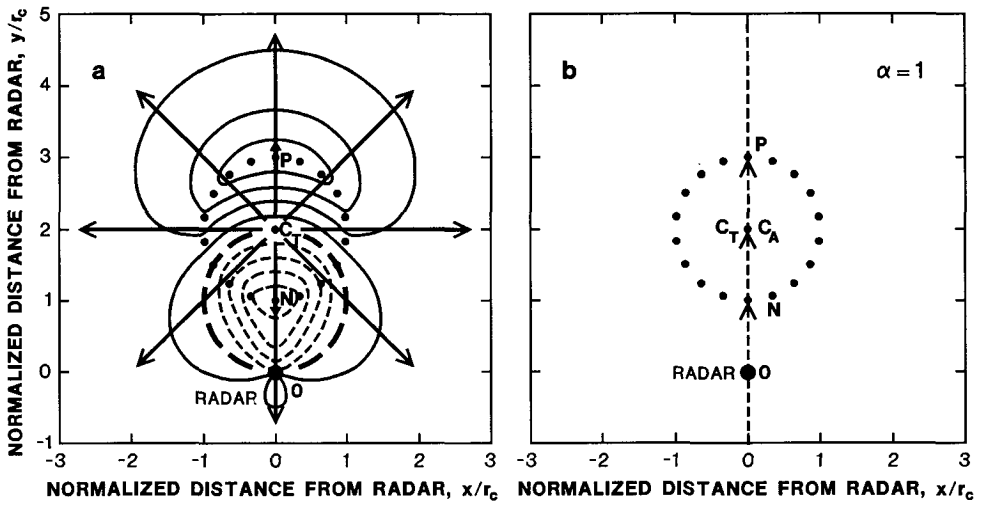

FIG. 4. Same as Fig. 2 except for axisymmetric divergent flow, as indicated by the thick streamlines. The solid circle representing the radar range circle is removed.

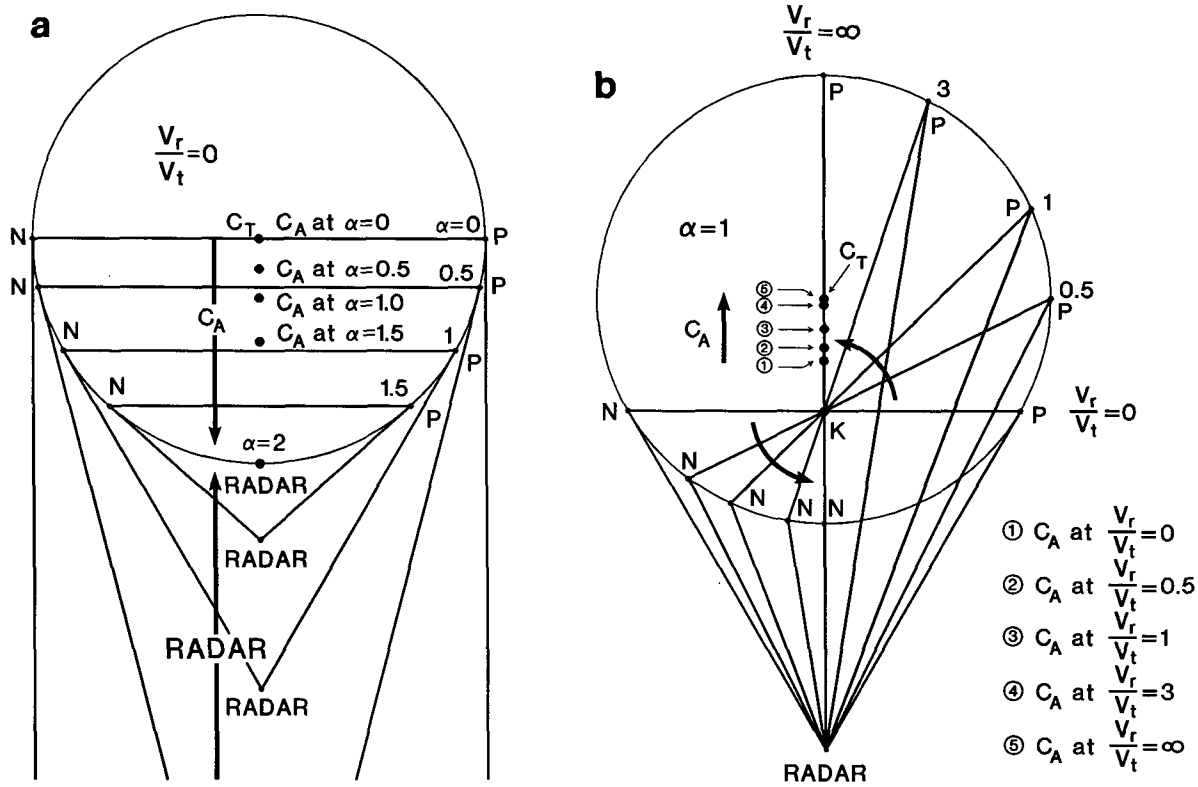

FIG. 5. Variation of signature with (a) variable aspect ratios for fixed velocity ratio of zero and (b) variable velocity ratios for fixed aspect ratio of one. The solid circle centered on the true circulation center C_T represents the circle of maximum winds. Point K is the intersection of chords NP with the line connecting the radar location and true center. The heavy arrows in (a) indicate the directions that the apparent center C_A and radar location move as the aspect ratio α increases. The heavy straight arrow in (b) indicates the direction that the apparent center moves as the velocity ratio increases. Other parameters are defined in the text.

The geometrical relationships used to derive the correction factor are shown in Fig. 6. The correction factor can be expressed in terms of the range and azimuth (R_N, θ_N) of the extreme negative Doppler velocity value and the range and azimuth (R_p, θ_p) of the extreme positive velocity value.

a. Aspect ratio

The aspect ratio α in (6) is defined in terms of true core diameter D_T and true range R_T as

$$\alpha \equiv \frac{D_T}{R_T}. \tag{10}$$

To redefine α in terms of measurable quantities, we use the following relationship, which is derived in appendix B:

$$\frac{D_T}{D_A} = \frac{R_T}{R_A}. \tag{11}$$

Rearranging terms, we have an expression for α in terms of measured quantities:

$$\alpha = \frac{D_A}{R_A}. \tag{12}$$

b. Core diameter

From the law of cosines applied to triangle ONP in Fig. 6, the apparent core diameter D_A is given by

$$D_A = (R_N^2 + R_P^2 - 2R_N R_P \cos\Delta\theta)^{1/2}, \tag{13}$$

where $\Delta\theta = \theta_P - \theta_N$ is the azimuth angle difference between the two peak Doppler velocity values ($\Delta\theta > 0$ for cyclonic circulation, $\Delta\theta < 0$ for anticyclonic circulation). As shown in Fig. 6, the true core diameter ($D_T = 2r_c$) of the dotted circle centered on C_T is given by $D_T = D_A \csc(\gamma/2)$, where γ is the angle subtended at C_T by the chord NP. Since the quadrilateral ONC_TP is cyclic (see appendix B), $\gamma = 180° - |\Delta\theta|$. Thus, $D_T = D_A \sec(\Delta\theta/2)$. The correction factor F can be estimated from the observed angle $\Delta\theta$ using the following relation:

$$F \equiv \frac{D_T}{D_A} = \frac{R_T}{R_A} = \sec\frac{\Delta\theta}{2}, \quad 0° \leq |\Delta\theta| < 180°. \tag{14}$$

The estimated core diameter D_E of the flow feature is given by

$$D_E = FD_A, \tag{15}$$

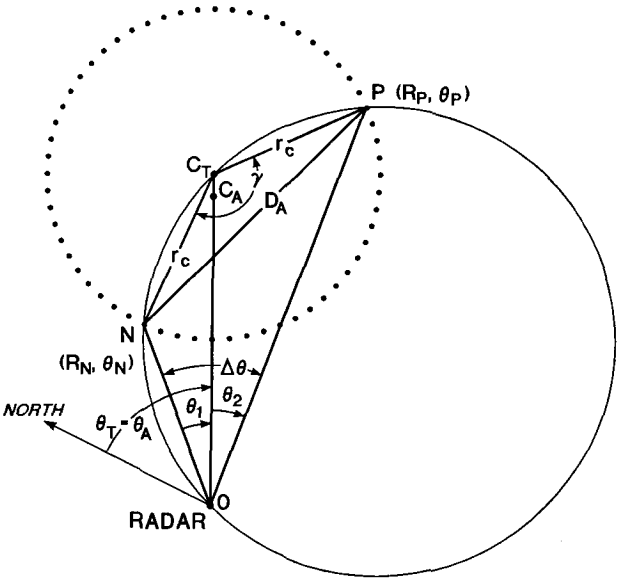

FIG. 6. Geometry for determining relationships between apparent (D_A) and true ($D_T = 2r_c$) core diameters and between apparent (C_A) and true (C_T) circulation centers. Extreme negative and positive Doppler velocity values at the core radius r_c occur, respectively, at N and P on the dotted circle of maximum winds. Ranges (R_N, R_P) and azimuth angles (θ_N, θ_P) are the locations of peak Doppler velocity values. The solid circle passes through the radar location O, points N and P, and true circulation center C_T. At the radar location O, $\Delta\theta = (\theta_P - \theta_N)$ is the azimuth angle difference between N and P.

where the subscript E indicates an estimate of the true value.

c. Center range and azimuth

As mentioned in section 3a, the apparent range R_A from the radar to the apparent center C_A is defined as the average of R_N and R_P, given by

$$R_A = \frac{R_N + R_P}{2}. \tag{16}$$

The estimated true range R_E to the feature center is represented by

$$R_E = FR_A, \tag{17}$$

where F is the correction factor.

The true (θ_T) and apparent (θ_A) azimuths of the signature center are defined, respectively, as the angle (positive in a clockwise direction) at the radar location between north and the radar range to the true (C_T) and apparent (C_A) centers (Fig. 6). Since OC_T and OC_A lie along the same radial direction from the radar, $\theta_T = \theta_A$. To determine the value of θ_A, consider the inscribed triangles, NOC_T and POC_T, in Fig. 6. Since chords NC_T and PC_T are both equal to the core radius r_c, the opposite inscribed angles, θ_1 and θ_2, are equal. Thus, the azimuth of chord OC_T, which bisects $\Delta\theta$, is midway between θ_N and θ_P. The true azimuth of the signature center from the radar then can be estimated from

$$\theta_E = \theta_A \equiv \frac{\theta_N + \theta_P}{2}. \tag{18}$$

5. Application to atmospheric vortices

How can we determine at what ranges the distortions become important for various atmospheric phenomena ranging from mesocyclones to hurricanes? This question can be answered by plotting the correction factor F that, for the special case of axisymmetric rotation only, can be expressed in terms of apparent core diameter and apparent range through the aspect ratio relationship

$$\alpha = \frac{D_T}{R_T} = \frac{D_A}{R_A} = 2\sin\frac{\Delta\theta}{2}, \quad \text{(rotation only)} \tag{19}$$

where $\Delta\theta/2 = \cos^{-1}(F^{-1})$. The corresponding correction factor curves are plotted in Fig. 7. According to (19), these curves apply to both true diameter and range and apparent diameter and range. As a flow feature moves from infinite range to a distance from the radar equal to the core radius, the correction factor increases from one to infinity.

Let us consider an idealized hurricane having an apparent core diameter of 50 km at an apparent range

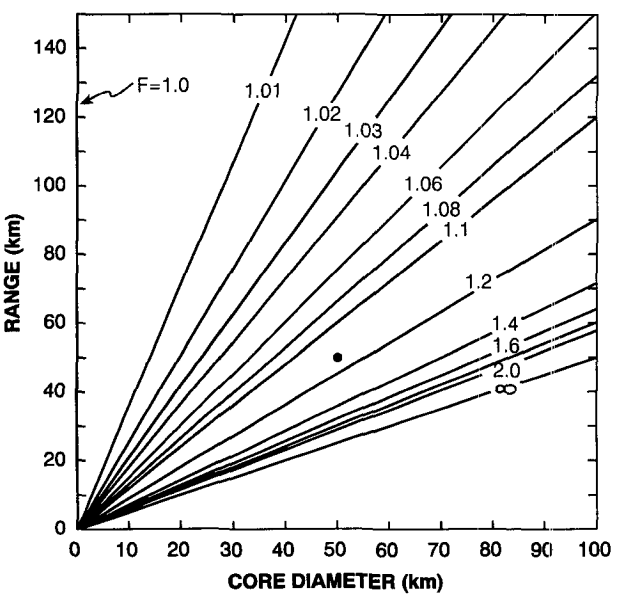

FIG. 7. Plot of correction factor F as a function of core diameter and radar range to feature center for the case of axisymmetric rotation only. The correction factor applies to both true and apparent values. The heavy dot is an example for a hurricane having an apparent core diameter of 50 km at an apparent range of 50 km from a Doppler radar.

of 50 km from a Doppler radar, as indicated by a heavy dot in Fig. 7. For aspect ratio of 1, the correction factor is found to be 1.15; the corresponding azimuth-angle difference between the two peak Doppler velocity values is 60°. Based on (14), this correction factor indicates that both the apparent range and apparent core diameter are in error by about 8 km. The curves in Fig. 7 indicate that, as a hurricane continues to approach the radar, the correction factor increases in an exponential manner.

In severe thunderstorms, the effect of Doppler radar range on mesocyclones is insignificant. For instance, a mesocyclone having a typical core diameter of 5 km would have to be within 5 km of the radar for the correction factor to be 1.15 or greater. Moving at 12 m s^{-1}, a mesocyclone would be within the 5-km range for less than 14 min. Since this time period is short and it is extremely rare for a mesocyclone to be within 5 km of a radar, the correction factor does not play an important role in the routine real-time interpretation of mesocyclone characteristics.

6. Conclusions

Geometrical and mathematical relationships are presented that describe the variation in the single-Doppler velocity patterns of quasi-axisymmetric rotation and divergence regions as a function of radar range. The velocity patterns become distorted as they approach a Doppler radar site. Distortion is a function of the aspect ratio (ratio of core diameter to range of a feature center from the radar) and a function of the velocity ratio (ratio of peak radial velocity to peak tangential velocity), where the apparent core diameters and locations of the pattern centers depart from their true values as the aspect ratio increases and the velocity ratio approaches zero. Adding convergence (divergence) to a purely cyclonic circulation causes a clockwise (counterclockwise) shift of the Doppler velocity peaks and distortion of the Doppler velocity patterns relative to cyclonic rotation alone. Deviations of the apparent core diameters and locations of the flow-feature centers from their true values can be estimated using a correction factor. The correction factor F represents the ratio of true to apparent core diameters D_T/D_A, as well as the ratio of true to apparent radar ranges to the core center R_T/R_A. The correction factor increases from one to infinity as a flow feature moves from infinite range to a distance from the radar equal to the core radius. The true and apparent centers occur at the same azimuth from the radar. For the pure divergence–convergence case, D_A and R_A always are equal to D_T and R_T, respectively, regardless of the flow-feature size and range from the radar.

As a core of pure rotation is transformed into one of pure divergence at a given range, the chord D_A connecting the points of maximum and minimum Doppler velocity values, initially perpendicular to the radar viewing direction, rotates until it becomes parallel to the viewing direction. At the same time, the location of the apparent center moves toward the true center of the Doppler velocity signature.

The problem of velocity-pattern distortion is most critical for large-scale vortices, such as hurricanes. The apparent diameter and center position become increasingly in error as the region of maximum winds approaches coastal population centers. On the thunderstorm scale, distortion effects are not important, because the typical mesocyclone would have to be within 5 km of the radar before position errors would be significant.

The addition of uniform wind to an axisymmetric disturbance does not alter the results presented in this paper. In Brown and Wood (1991), we pointed out that such an addition changes Doppler velocity values but does not change the Doppler velocity *pattern*.

The techniques developed in this paper are based on quasi-horizontal measurements of features that are axisymmetric about a vertical axis. In nature, vortices are not precisely axisymmetric, but they are close enough for the basic techniques to apply. The primary requirement is that this approach be applied to data collected at low elevation angles.

Equations used to estimate the true characteristics of the features have been applied elsewhere to two-dimensional, horizontal, gridded Hurricane Alicia (1983) wind data, which were reconstructed from in situ aircraft measurements (Wood 1991). The calculations of estimated core diameters and estimated signature center positions from the radar indicated that the equations work well for quasi-axisymmetric, intense storms. Single-Doppler radar alone cannot determine the total extent of wind asymmetries because the radar measures only the radial component of velocity along the radar viewing direction.

7. Future research

Knowledge of the results presented in this paper should be helpful when a hurricane approaches a coastline where a future WSR-88D radar (initially known as Next Generation Weather Radar, NEXRAD) is operating. Based on a study of Hurricane Frederick (1979), Marks (1990) found that the reflectivity-based radar center of the hurricane usually was different than the airborne Doppler-derived wind center. The radar center was determined from the centroid of the oval reflectivity maximum. The wind center often was observed closer to the more intense portion of the eyewall reflectivity maximum. In view of uncertainties of flow-field asymmetries on range-related distortions for hurricanes nearing land, it is recommended that more studies be undertaken of Doppler radar measurements within hurricanes.

Acknowledgments. The authors thank Don Burgess and Drs. Robert Davies-Jones and Thomas Matejka for their suggestions and assistance during this study. We appreciate the thorough reviews of and helpful suggestions from two anonymous reviewers. Joan Kimpel skillfully produced the figures.

APPENDIX A

Derivation of Doppler Velocity Values for Axisymmetric Flow Fields

The purpose of this appendix is to derive (3). With respect to the center of an axisymmetric circulation, the vector velocity **V** is expressed as

$$\mathbf{V} = v_r\mathbf{e}_r - v_t\mathbf{e}_t, \tag{A1}$$

where

$$\mathbf{e}_r \equiv \sin\beta\mathbf{i} + \cos\beta\mathbf{j}, \tag{A2}$$

$$\mathbf{e}_t \equiv \cos\beta\mathbf{i} - \sin\beta\mathbf{j}. \tag{A3}$$

Here, unit vectors $\mathbf{e}_r$ and $\mathbf{e}_t$, written in terms of geographical unit vectors **i** and **j**, point, respectively, in the direction of the radial (v_r) wind component and in the opposite direction of the cyclonic tangential (v_t) wind component of the flow feature centered at C_T, as shown in Fig. A1. Here β is defined as the angle (positive in a clockwise direction) between north and the radial direction from the axisymmetric circulation center C_T.

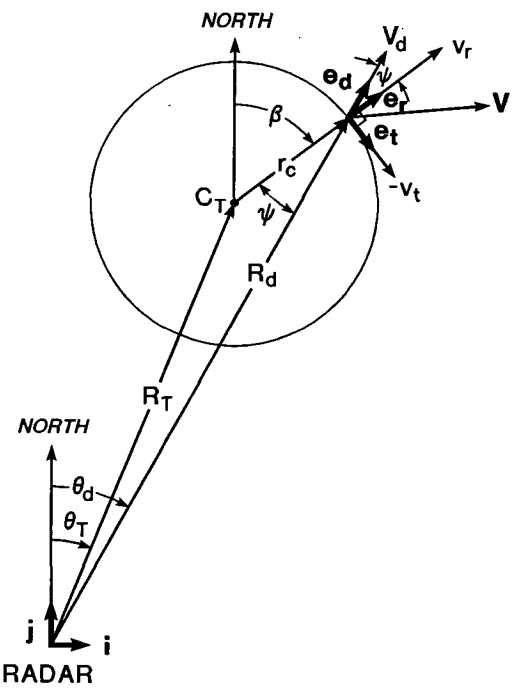

FIG. A1. Geometry for computing Doppler velocity V_d at a point (R_d, θ_d) relative to a true circulation center C_T at (R_T, θ_T).

The Doppler velocity value V_d is calculated from the radial (v_r) and tangential (v_t) wind components of the axisymmetric circulation by taking the dot product of (A1) with $\mathbf{e}_d$,

$$V_d = \mathbf{V}\cdot\mathbf{e}_d, \tag{A4}$$

where

$$\mathbf{e}_d = \sin\theta_d\mathbf{i} + \cos\theta_d\mathbf{j}. \tag{A5}$$

Here $\mathbf{e}_d$ is a unit vector in the direction of V_d; θ_d is defined in (5). From (A1) through (A5), it follows that

$$V_d = v_r\cos\psi + v_t\sin\psi, \quad -\pi \leq \psi \leq \pi, \tag{A6}$$

where $\psi\ (\equiv\beta - \theta_d)$ is the angle between the radar viewing direction and the radial direction from the center of the axisymmetric circulation. The angle ψ can be expressed in terms of the range and azimuth in Fig. A1, using the cosine and sine rules (Jendrowski 1986),

$$\cos\psi = \frac{R_d - R_T\cos(\theta_d - \theta_T)}{r}, \tag{A7}$$

$$\sin\psi = \frac{R_T\sin(\theta_d - \theta_T)}{r}, \tag{A8}$$

where R_T, θ_T represents the range and azimuth of the axisymmetric circulation center C_T. Therefore, with aid of (1), (2), (A7), and (A8), (A6) becomes

$$V_d = \left(\frac{r}{r_c}\right)^{\lambda-1}\left\{V_r\left[\frac{R_d - R_T\cos(\theta_d - \theta_T)}{r_c}\right] + V_t\frac{R_T}{r_c}\sin(\theta_d - \theta_T)\right\}. \tag{A9}$$

APPENDIX B

Derivation of Expression Relating True and Apparent Diameters and Radar Ranges

We need to redefine the aspect ratio (α) in (10) in terms of the measurable quantities D_A, R_N, and R_P. To do this, we make use of the geometric relationships in Fig. 6. Using the law of cosines, we obtain two expressions for D_A from two adjacent triangles, C_TNP and ONP, such that

$$D_A^2 = \frac{D_T^2}{2}(1 - \cos\gamma), \tag{B1}$$

$$D_A^2 = R_N^2 + R_P^2 - 2R_NR_P\cos\Delta\theta, \tag{B2}$$

where $D_T = 2r_c$. Since ON, NC_T, C_TP, and PO are all chords of the solid circle, ONC_TP is a cyclic quadrilateral (Gellert et al. 1977, p. 176). Accordingly, the sum of opposite angles γ and $|\Delta\theta|$ is equal to 180°. Since $\cos\gamma = -\cos\Delta\theta$, combining (B1) and (B2) to eliminate $\cos\Delta\theta$,

$$D_A^2 = \frac{D_T^2 R_A^2}{(D_T^2/4) + R_N R_P}, \quad \text{(B3)}$$

where R_A [$\equiv(R_N + R_P)/2$] is the apparent range. We now show that the denominator on the right-hand side of (B3) is equal to R_T^2 by using the law of cosines on adjacent triangles ONC_T and OPC_T. That is,

$$R_T^2 = \frac{D_T^2}{4} + R_N^2 - D_T R_N \cos(\angle ONC_T), \quad \text{(B4)}$$

$$R_T^2 = \frac{D_T^2}{4} + R_P^2 - D_T R_P \cos(\angle OPC_T). \quad \text{(B5)}$$

Using the same approach in obtaining (B3) and combining (B4) and (B5) to eliminate $\cos(\angle ONC_T)$ and $\cos(\angle OPC_T)$, one finds that

$$R_T^2 = \frac{D_T^2}{4} + R_N R_P. \quad \text{(B6)}$$

Thus, (B3) becomes, with the aid of (B6),

$$\frac{D_T}{D_A} = \frac{R_T}{R_A}. \quad \text{(B7)}$$

REFERENCES

Baynton, H. W., 1979: The case for Doppler radars along our hurricane affected coasts. *Bull. Amer. Meteor. Soc.*, **60,** 1014–1023.

Brown, R. A., and V. T. Wood, 1983: Improved severe storm warnings using Doppler radar. *Natl. Wea. Dig.*, **8**(3), 17–27; errata, 1984: **9**(1), 20.

——, and ——, 1991: On the interpretation of single-Doppler velocity patterns within severe thunderstorms. *Wea. Forecasting*, **6,** 32–48.

——, L. R. Lemon, and D. W. Burgess, 1978: Tornado detection by pulsed Doppler radar. *Mon. Wea. Rev.*, **106,** 29–38.

Burgess, D. W., 1976: Single-Doppler radar vortex recognition: Part I. Mesocyclone signatures. Preprints, *17th Conf. on Radar Meteorology,* Seattle, Amer. Meteor. Soc., 97–103.

Donaldson, R. J., Jr., 1970: Vortex signature recognition by a Doppler radar. *J. Appl. Meteor.*, **9,** 661–670.

Eilts, M. D., and R. J. Doviak, 1987: Oklahoma downbursts and their asymmetry. *J. Appl. Meteor.*, **26,** 69–78.

Fujita, T. T., 1985: The downburst: Microburst and macroburst. SMRP Research Paper No. 210, University of Chicago, 122 pp.

Gellert, W., H. Küstner, M. Hellwich, and H. Kästner, 1977: *The VNR Concise Encyclopedia of Mathematics.* Van Nostrand Reinhold Company, 760 pp.

Gray, W. M., and D. J. Shea, 1973: The hurricane's inner core region. Part II. Thermal stability and dynamic characteristics. *J. Atmos. Sci.*, **30,** 1565–1576.

Houze, R. A., Jr., S. A. Rutledge, M. I. Biggerstaff, and B. F. Smull, 1989: Interpretation of Doppler weather radar displays of midlatitude mesoscale convective systems. *Bull. Amer. Meteor. Soc.*, **70,** 608–619.

Jendrowski, P. A., 1986: Performance of quantitative parameters associated with the NEXRAD mesocyclone detection algorithm from simulated single-Doppler velocities. M. S. thesis, Department of Meteorology, University of Maryland, 123 pp. [Available from University of Maryland Library, College Park, MD 20742.]

Lemon, L. R., and D. W. Burgess, 1980: Magnitude and implications of high speed outflow at severe storm summits. Preprints, *19th Conf. on Radar Meteorology,* Miami Beach, Amer. Meteor. Soc., 364–368.

Marks, F. D., Jr., 1990: Radar observations of tropical weather systems. *Radar In Meteorology,* D. Atlas, Ed., Amer. Meteor. Soc., 401–425.

Rankine, W. J. M., 1901: Motions of fluids. *A Manual of Applied Mechanics,* 16th ed., Charles Griff and Company, 574–578.

Shea, D. J., and W. M. Gray, 1973: The hurricane's inner core region. Part I. Symmetric and asymmetric structures. *J. Atmos. Sci.*, **30,** 1544–1564.

Wilson, J. W., and K. E. Wilk, 1982: Nowcasting applications of Doppler radar. *Nowcasting,* K. A. Browning, Ed., Academic Press, 87–105.

——, R. D. Roberts, C. Kessinger, and J. McCarthy, 1984: Microburst wind structure and evaluation of Doppler radar for airport wind shear detection. *J. Appl. Meteor.*, **23,** 898–915.

Witt, A., and S. P. Nelson, 1991: The use of single-Doppler radar for estimating maximum hail size. *J. Appl. Meteor.*, **30,** 425–431.

Wood, V. T., 1991: Objective determination of tropical cyclone tracks from land-based Doppler radar observations. Preprints, *19th Conf. on Hurricanes and Tropical Meteorology,* Miami, Amer. Meteor. Soc., 198–201.

——, and R. A. Brown, 1986: Single-Doppler velocity signature interpretation of nondivergent environmental winds. *J. Atmos. Oceanic Technol.*, **6,** 114–128.

——, and F. D. Marks, Jr., 1989: Hurricane Gloria: Simulated land-based Doppler velocities reconstructed from airborne Doppler radar measurements. Preprints, *18th Conf. on Hurricanes and Tropical Meteorology,* San Diego, Amer. Meteor. Soc., 115–116.